Journal of Solid State Chemistry **158,** 198–207 (2001)
doi:10.1006/jssc.2001.9093, available online at http://www.idealibrary.com on IDEAL®

Unexpected Spin–Glass Behavior of the Mixed Sulfide-Selenide Chalcogenides $TlCr_5S_{8-y}Se_y$ ($y = 1$–7) Mediated by the Nonmagnetic Sublattice

W. Bensch and B. Sander

Institut für Anorganische Chemie, CAU Kiel, Olshausenstrasse 40, D-24098 Kiel, Germany

R. K. Kremer

Max Planck Institut für Festkörperforschung, Heisenbergstrasse 1, D-70506 Stuttgart, Germany

and

W. Kockelmann[1]

Mineralogisch–Petrologisches Institut, Universität Bonn, D-53115 Bonn, Germany

Received August 10, 2000; in revised form December 14, 2000; accepted January 19, 2001

Spin–glass behavior in the series $TlCr_5S_{8-y}Se_y$ is mediated by the nonmagnetic anionic sublattice. The magnetic susceptibilities of compounds with $1 \le y \le 8$ follow a Curie–Weiss law in the high temperature region above 300 K. As the Se content increases, the magnitude of the Weiss constant θ drastically decreases from about $-499(3)$ K for $TlCr_5S_7Se$ to $-180(3)$ K for $TlCr_5Se_8$. Substitution of S by Se leads to structural alterations and stronger ferromagnetic exchange interactions according to the well-established Goodenough–Kanamori rules. In the low-temperature region, zero field cooled and field cooled susceptibility curves split below a characteristic freezing temperature T_f, which increases with rising Se content from 23 to 46 K for $TlCr_5SeS_7$ to $TlCr_5Se_7S$, respectively. Using an Ising spin model, the magnetic frustration and the observed spin–glass behavior can be explained by considering different ferromagnetic and antiferromagnetic exchange paths. Neutron diffraction patterns at 5 K show no long-range magnetic order. Analyses of broad humps of magnetic scattering in the diffraction patterns in terms of real space distribution functions show that the antiferromagnetic exchange becomes weaker at the expense of increasing ferromagnetic correlations between 120 and 5 K. Nonlinear changes of θ, T_f, and the effective magnetic moment per Cr(III) across the $TlCr_5S_{8-y}Se_y$ series, but linear dependencies of T_f and θ on composition within the two regions $1 \le y \le 4$ and $4 \le y \le 7$ in the low and high temperature regimes, respectively, indicate that a critical Cr–Cr interatomic distance is reached at $y \approx 4$.

[1]Present address: ISIS Facility, Rutherford Appleton Laboratory, Chilton, OX11 0QX, UK.

INTRODUCTION

A large number of compounds with the composition AM_5X_8 (A = K, Rb, Cs, Tl, In, Eu, Sn; M = Ti, V, Nb, Cr; X = S, Se, Te) crystallize with the TlV_5S_8-type structure reflecting its wide flexibility (1–16). Depending on the transition metal in AM_5X_8, interesting physical properties were reported. Several groups investigated the nature of bonding between the guest atom Tl and the host matrix V_5S_8 of the metallic paramagnet $Tl_xV_5S_8$ (17–25). The relation between the crystal structures and the physical properties were also studied for $TlCr_5Se_8$ (12, 14, 26–29), $A_xNb_5Se_8$ (A = Sn, Eu, Pb; $x \approx 0.6$) (10), and $TlV_{5-y}Fe_yS_8$ (30). The distinct character of the d electrons of V and Cr and its effects on the crystal structures, electronic band structures, as well as magnetic properties were investigated in the $TlV_{5-y}Cr_yS_8$ series (31–34). The two ternary chromium chalcogenides $Tl_xCr_5S_8$ and $Tl_xCr_5Se_8$ exhibit very different chemical and physical properties (27–29, 35, 36). In the sulfide, the magnetic behavior is dominated by a Cr_2-dimer (Cr2–Cr3 across common face), identified from the typical temperature dependence of the magnetic susceptibility of a $S = \frac{3}{2}$ dimer (36). The selenide shows normal Curie–Weiss-like behavior with a transition into an antiferromagnetic state at $T_N \cong 50$ K (14, 27, 37). One highly interesting feature of the crystal structures is the short Cr–Cr interatomic distance being only slightly enlarged when S is fully substituted by Se (2.959 vs 3.058 Å, Cr2–Cr3 across common faces of the Se octahedra). The other Cr–Cr distances across common edges are significantly enlarged when

0022-4596/01 $35.00

S is replaced by Se. It can be assumed that the small increase of the Cr2–Cr3 distance together with the higher polarizability of Se are responsible for the significantly different magnetic properties of the two end members of the series.

Until recently, all investigations were focused either on the influence of the nature and concentration of the guest atoms A in AM_5X_8 onto the resulting structural and physical properties or they were concerned with the study of the effects when the metal atoms are changed.

Recently, we reported the preparation and crystal structures of $TlCr_5S_{8-y}Se_y$ ($y = 1$–7) (38). The most interesting results of the investigations can be summarized as follows: The four crystallographic independent sites for the chalcogen atoms are occupied in an unexpected preferential fashion. Over the whole series, the Se atoms prefer the two sites with the largest number of Tl atoms as nearest neighbors and the highest coordination number. For one site, no significant preference was found, and the fourth site is clearly less favored by the Se atoms. This preferential occupation leads to an unexpected and spectacular dependence of the unit-cell parameters and of the interatomic distances as function of the Se content. The **a** axis shows a negative deviation from linearity (Vegards law), whereas the **c** axis exhibits a positive deviation. The monoclinic angle β passes a maximum at $y = 5$ and finally drops to a value comparable with that obtained for the pure sulfide. It was demonstrated that the series can be divided into the two different regions $0 \leq y \leq 4$ and $5 \leq y \leq 8$, both characterized by a linear variation of the lattice parameters as well as of the interatomic distances.

The magnetic properties of the different members of the series $TlCr_5S_{8-y}Se_y$ ($1 \leq y \leq 7$) should sensitively reflect the changes of interatomic Cr–Cr distances, Cr–X–Cr angles, and the different polarizabilities of the anions and provide additional information about the bonding properties. In addition, the experiments give evidence whether the magnetic properties vary in a more or if less smooth fashion or if an abrupt change occurs at a "critical" composition associated with a distinct critical Cr–Cr distance.

EXPERIMENTAL DETAILS

The samples were prepared by heating stoichiometric amounts of the elements at 1000°C. The exact conditions are reported elsewhere (38). The homogeneity of all samples was checked with X-ray powder diffractometry, STOE STADI P, monochromatized Cu$K\alpha$ radiation, $\lambda =$ 1.54056 Å. The magnetic susceptibility measurements were performed on a Quantum design MPMS7 magnetometer at two different fields of 100 and 1000 G. Zero field cooling (zfc) and field cooling (fc) experiments were performed in the usual way. The high-temperature investigations were performed on a Faraday balance at a field of 1.5 T. The raw data were corrected for core diamagnetism using Pascals increments. Neutron scattering experiments were done between 5 and 300 K on the ROTAX instrument at ISIS (39). Rietveld refinements were performed with the GSAS package (40). Refinement results are summarized in Table 1. The profiles were modeled with a double-exponential Voigt function using 10 parameters. The background was treated with 22 parameters, and in total 55 parameters were refined.

TABLE 1
Results of Rietveld Refinement of $TlCr_5Se_2S_6$
Neutron Data at 300 K

a [Å]		b [Å]	c [Å]	β [Å]		
17.9571(5)		3.4693(1)	8.7166(2)	105.144(2)		
[17.9772]		[3.4752]	[8.7242]	[105.128]		
		F	x	y	z	U_{iso} [Å^2]
Tl	4(i)	0.5	0.01135	0	− 0.00148	0.04133
Cr1	2(d)	1.0	0	0.5	0.5	0.01011
Cr2	4(i)	1.0	0.2051(4)	0	0.8302(6)	0.01096
			[0.20461]		[0.83267]	
Cr3	4(i)	1.0	0.1591(4)	0	0.4811(7)	0.01074
			[0.15782]		[0.48036]	
Se1	4(i)	0.403(8)	0.1658(3)	0.5	0.9923(7)	0.01304
		[0.40861]	[0.16633]		[0.99119]	
Se2		0.364(11)	0.0841(3)	0.5	0.3166(5)	0.01221
		[0.31196]	[0.08399]		[0.31896]	
Se3	4(i)	0.177(8)	0.2597(4)	0	0.3449(8)	0.01023
		[0.18084]	[0.26012]		[0.34219]	
Se4	4(i)	0.092(8)	0.0758(5)	0	0.659(1)	0.01067
		[0.08079]	[0.07505]		[0.65518]	

$R_{profile} = 2.3\%$ $R_{Bragg} = 5.5\%$

Note. The parameters in square brackets obtained from X-ray single crystal diffraction (38) are given for comparison. Parameters without Rietveld esd's (in parentheses) were kept fixed at values from X-ray single crystal diffraction. F is the site occupation factor; the occupation of sulfur is $F(S) = 1 - F(Se)$.

RESULTS AND DISCUSSION

A. High-Temperature Region

For a better understanding of the following discussions, the basic features of the crystal structure of $TlCr_5X_8$ are presented. In the structure, layers of Cr1- and Cr3-centered chalcogen octahedra sharing common edges are running parallel to the (001) plane and are connected by Cr2-centered double octahedra units via common faces leading to a three- dimensional network. Nearly rectangular channels parallel to [010] are occupied by the Tl atoms (see Fig. 1).

The high-temperature susceptibility data were fitted with a Curie–Weiss law (Table 2). We note that attempts to fit the data with a modified Curie–Weiss law including a contribution for a temperature independent paramagnetism (TIP) χ_0 always converges to negative values for χ_0(TIP).

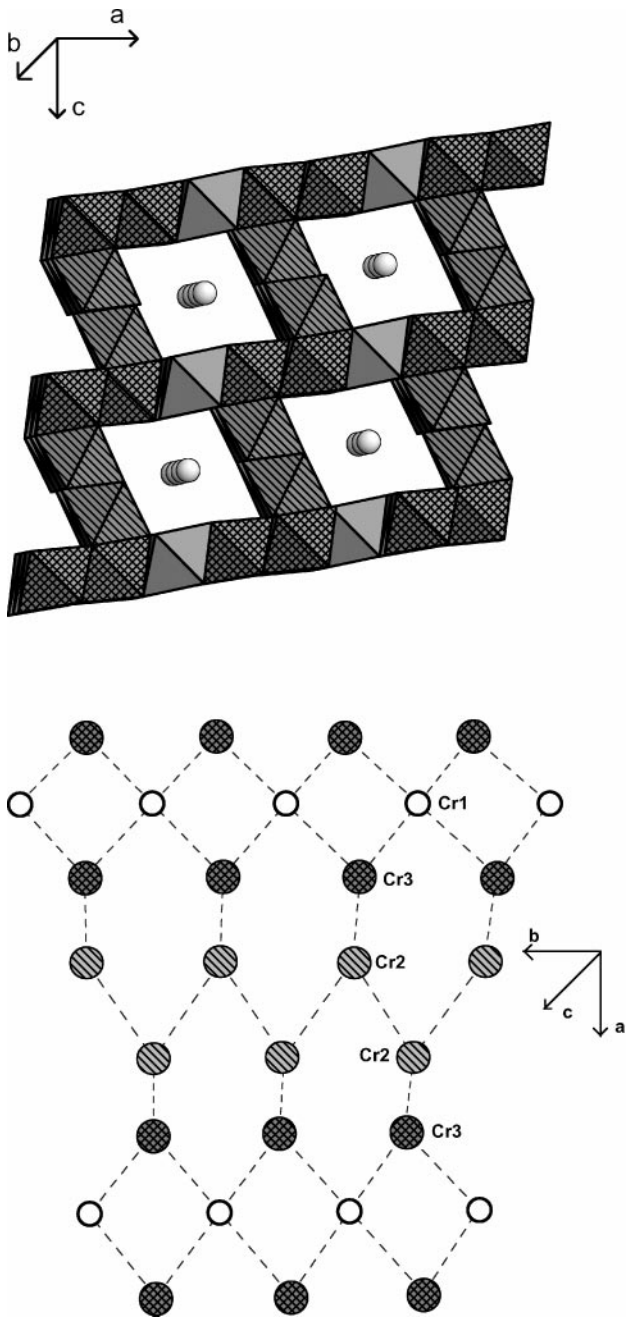

FIG. 1. (top) Polyhedral representation of the crystal structure of $TlCr_5Se_8$. The Cr(2)-centered octahedra are marked with lines, the Cr(3) octahedra are cross hatched. The gray spheres represent the Tl atoms within the channels. (bottom) The quasi-two-dimensional metal atom network is represented.

With increasing Se content the value for the paramagnetic Curie temperature drastically decreases from about $-499(3)$ K for $TlCr_5S_7Se$ to $-180(3)$ K for $TlCr_5Se_8$, suggesting stronger ferromagnetic exchange interactions in the Se richer compounds. The dependence of θ on the composition is displayed in Fig. 2. We note that for $TlCr_5Se_8$ slightly different θ values were reported (see Table 2 and Refs. (14, 37)). The differences may be due to the different temperature ranges used for the evaluation of θ (measurements only below 300 K) and the fitting with a Curie–Weiss law including a χ_0 term.

Based on the assumption that the spin state of Cr is not altered when S is substituted by Se it can be assumed that within the whole series Cr is in the Cr(III) d^3 spin state. Based on Goodenough's and Kanamori's model qualitatively describing the competition between direct cation–cation and indirect cation–anion–cation exchange (41–43), two different exchange pathways must be invoked to explain the magnetic behavior. First, the direct exchange interaction between neighboring Cr atoms located in the octahedra sharing common faces involving the half-filled t_{2g} levels of the Cr^{3+} ions leads to antiferromagnetic exchange with the strength of interaction depending sensitively on the Cr–Cr separation. The analysis of the magnetic properties of a large number of chromium chalcogenide spinels revealed that the strength of the direct exchange interactions is only substantial below a critical distance R_c of about 3.5 Å (44).

On the other hand, indirect 90° superexchange of the type Cr^{3+}–X^{2-}–Cr^{3+} involves a half-filled t_{2g} orbital of one cation, an empty e_g orbital of the second cation, and a doubly occupied p orbital of the anion, thus favoring ferromagnetic exchange. The ferromagnetic exchange becomes weaker with increasing deviation of the angle from 90°. Both mechanisms can occur simultaneously, the predominating type depending on the actual interatomic metal-to-metal distances and Cr–X–Cr angles.

Within the whole composition range for $TlCr_5S_{8-y}Se_y$ ($y = 0$–8) the Cr–Cr interatomic distances are below or near the value of 3.5 Å and increase when S is successively replaced by Se. Every CrX_6 octahedron is connected to two CrX_6 octahedra via common edges within the CrX_2 layers and has two additional CrX_6 octahedra above and below. The CrX_2 layers are joined by Cr_2X_{10} units composed of two edge-sharing CrX_6 octahedra via common faces. The possible interaction paths are schematically shown in Fig. 3. In total there are six possible ferromagnetic 90°Cr–X–Cr (J_f) and seven antiferromagnetic direct Cr–Cr (J_{af}) exchange paths.

It is obvious that a 90° superexchange mechanism is of less importance because our experimental results would be in contrast to what was reported for different chromium selenides of composition $MCrSe_2$ (M = Ag, Na, Hg, Cd) and for $CrSbSe_3$ (45, 46). These compounds exhibit ferromagnetic properties and the Cr–Cr distances are between 3.604 and 3.80 Å (45, 46). The distances are significantly longer than the critical R_c of about 3.5 Å and direct exchange can be neglected.

It must be assumed that the magnetic properties of the different compounds of the series $TlCr_5S_{8-y}Se_y$ ($y = 1$–7) in the high-temperature region are dominated by direct

TABLE 2
Magnetic Data for the High-Temperature Region for $TlCr_5S_{8-y}Se_y$ ($y = 1$–8)

y	0	1	2	3	4	5	6	7	8
μ/Cr [μ_B]	4.25	4.23	4.17	4.14	4.10	3.95	3.99	3.99	3.92
θ [K]	−568(4)	−499(3)	−432(3)	−386(3)	−330(3)	−288(3)	−250(3)	−202(2)	−180(3)

Compound	θ [K]	μ_{eff}/Cr [μ_B]	χ (TIP) 10^{-6} [emu/g]	Ref.
$TlCr_5Se_8$	−218	4.01	1.76	(37)
$InCr_5Se_{7.8}$	−233	4.2	0.72	(37)
$KCr_5Se_{7.8}$	−171	4.46	−2.2	(37)
$TlCr_5Te_{7.8}$	70	2.65	—	(37)
$TlCr_5Se_8$	−218	4.04	0.991	(14)
$Tl_{0.65}Cr_5Se_8$	−207	3.69	3.13	(14)
$Tl_{0.33}Cr_5Se_8$	−90.8	3.96	—	(14)
$TlCrS_2$	120	3.59	—	(51)
$TlCrSe_2$	130	3.71	—	(51)
$TlCrTe_2$	91	4.47	—	(51)
$TlCr_3S_5$	−259	3.43	—	(51)
$TlCr_3Se_5$	−156	2.79	—	(51)
$AgCrO_2$	−211	3.96	—	(51)
$Cr_2Sn_3Se_7$	3.26	3.65	—	(52)
$V_{0.9}Cr_{0.1}Se$	−1482	12.85	—	(53)
$V_{0.17}Cr_{0.83}Se$	48	3.74	—	(53)
$LaCrS_3$	−390	3.9	—	(54)
$Gd_{2/3}Cr_2S_4$	8	—	—	(55)
$CrSbSe_3$	150	4.0	—	(46)
$CrSiTe_3$	—	3.58		(56)

Note. Estimated standard deviations for θ are given in parentheses. Magnetic data for different Cr chalcogenides compiled from the literature are listed for comparison.

Cr^{3+}–Cr^{3+} interactions between the Cr atoms. The strong decrease of the Weiss constant with increasing Se content implies that the lengthening of *all* Cr–Cr separations is the essential structural feature determining the magnetic properties. With increasing Se content, the Cr2–Cr3 distance across the common face increases from 2.963 Å ($y = 1$) to 3.040 Å ($y = 7$), the two distances Cr1–Cr3 and Cr2–Cr2 between octahedra sharing common edges are enlarged from 3.350 to 3.464 Å and from 3.381 to 3.509 Å, respectively. It must be stressed that the Cr–Cr interatomic distances do not vary in a linear fashion and two different regions with linear dependence $y = 0$–4 and $y = 5$–8 can be distinguished (38). The nonlinear change of the Cr-Cr separations may be responsible for the observed nonlinear evolution of the Weiss constant θ with composition. The θ vs composition curve (compare Fig. 2) can, however, be divided into two regimes $0 < y < 4$ and $4 < y < 8$ with a linear change of θ in each region.

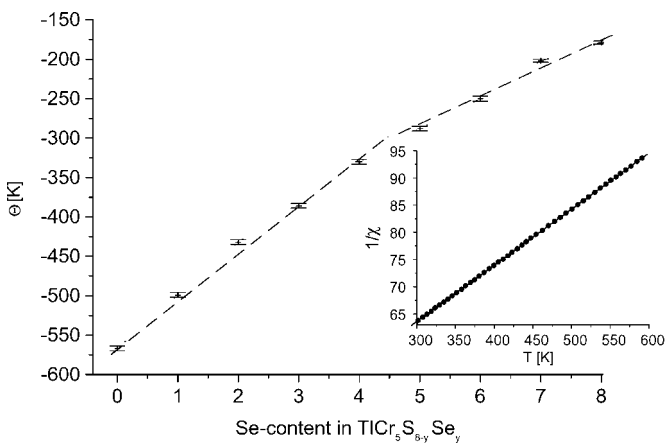

FIG. 2. Change of the Weiss constant θ with composition in $TlCr_5S_{8-y}Se_y$. The vertical bars represent the estimated standard deviations. The dotted line serves as a guide for the eyes. The inset shows a $1/\chi$ [mole/emu.] vs T plot for $TlCr_5S_4Se_4$: (black dots) experimental data, (thin line) Curie–Weiss fit.

Furthermore, the ferromagnetic 90° superexchange acts against the antiferromagnetic direct exchange, and it is well known that the former kind of exchange interaction is more effective when the anions are "softer" and more polarizable. Within the series, the hard S^{2-} anions are substituted by the softer Se^{2-} anions and the ferromagnetic 90° superexchange becomes more effective, thus weakening the net antiferromagnetic exchange.

In summary, there are at least two different counteracting effects which determine the magnitude of θ: Direct

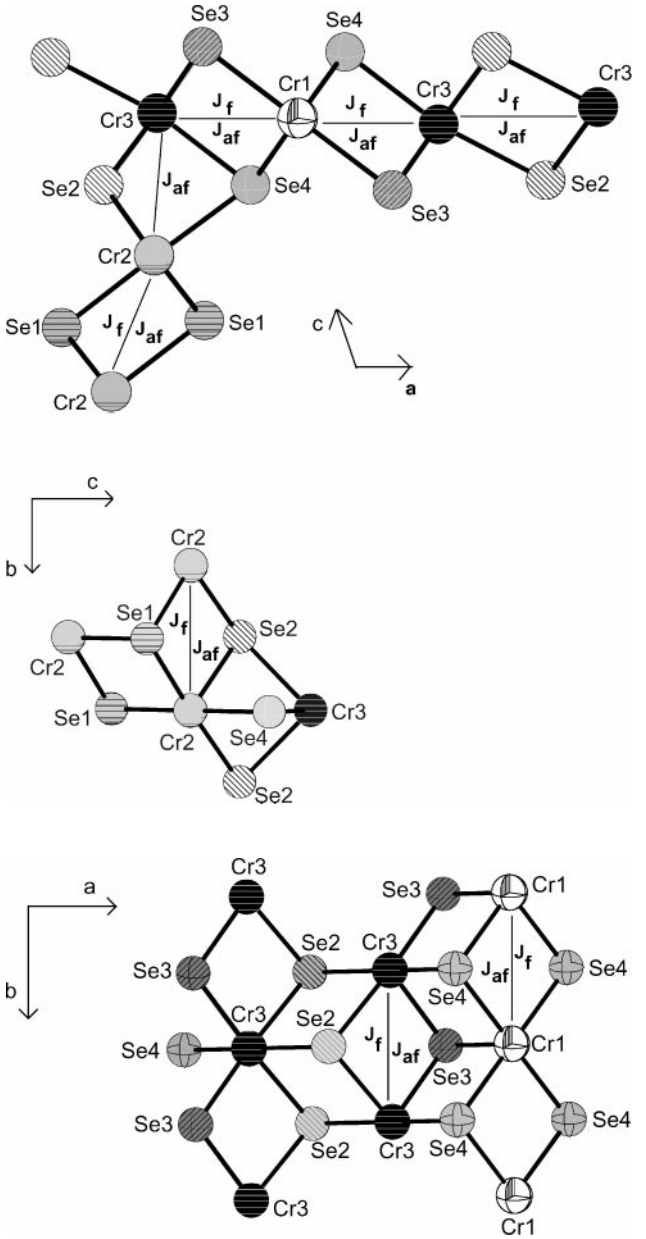

FIG. 3. Possible pathways for exchange interactions. *Note*: J_f and J_{af} means ferro- and antiferromagnetic exchange.

antiferromagnetic Cr–Cr exchange with $d(\text{Cr–Cr}) \leq \approx 3.5$ Å becomes less pronounced when S is replaced by Se, and the more effective indirect ferromagnetic 90° superexchange further reduces the magnitude of θ.

The calculated effective magnetic moments per Cr(III) d^3 are larger than the spin-only value of 3.87 μ_B and a continuous but nonlinear increase is found with increasing S content. The strongest change for μ_{eff}/Cr of about 0.15 μ_B occurs between the two adjacent compounds $y = 4$ and $y = 5$.

To give a possible explanation for this finding two observations must be considered giving evidences that the Cr–Cr interatomic distances are more important than the Cr–X–Cr angles for the determination of the magnetic behavior. The pure selenide is a three-dimensional antiferromagnet with $T_N = 55$ K (14, 27, 37). The magnetic spin structure was established by neutron scattering experiments (47). The spins located on Cr2 and Cr3 (common face, distance 3.058 Å at 300 K) are antiparallel. The magnetic exchange interaction between Cr2–Cr2 (3.516 Å at 300 K) leads to a collinear arrangement. These two spin arrangements require that the spins on Cr1 are either parallel or antiparallel oriented with respect to the orientation of the spin located on Cr3 (Cr1–Cr3: 3.493 Å at 300 K) (47). For the other end member of the solid solution the magnetic properties are clearly dominated by a Cr_2 dimer (Cr2–Cr3 = 2.898 Å) being in the antiferromagnetic ground state (36). Hence, the Cr2–Cr3 distance in $TlCr_5Se_8$ seems to be too long for the formation of such an antiferromagnetically coupled Cr_2 dimer, in the pure sulfide it is short enough. Recalling that all structural data revealed that the solid solution can be divided into two regions (see above) we assume that a critical Cr2–Cr3 distance is reached between $y = 4$ and 5; i.e., near this composition the Cr2–Cr3 separation is short enough to enable an antiferromagnetically coupled Cr_2 dimer. Consequently, a Curie–Weiss fit does not adequately describe the high-temperature magnetic properties of the compounds with a S content ≥ 5, and too large effective magnetic moments are obtained (see below).

At the end of this section we want to note that magnetic moments of about 4 μ_B/Cr(III) are often found in chromium chalcogenides, and several examples are included in Table 2.

B. Low-Temperature Region

As pointed out in the experimental section, the samples were first measured in the zfc mode and then in the fc mode. The temperature dependence of the magnetic susceptibilities of the different compounds are shown in Fig. 4. Surprisingly, the zfc and fc curves split below about 50 K. The temperature at which the splitting occurs depends on composition and amounts to 46 K for $TlCr_5Se_7S$ and to 23 K for $TlCr_5SeS_7$; i.e., the temperature increases with increasing Se content. Above this temperature the fc and zfc curves match perfectly onto each other. The splitting is reminiscent of spin–glass behavior, the temperature at which the splitting between fc and zfc susceptibility occurs determines the "freezing" temperature T_f. The variation of T_f with composition is displayed in Fig. 5. At temperatures below T_f, spins are frozen in metastable states. The apparent T_f depends on the magnitude of the magnetic field (see Figs. 5 and 6). A nearly linear change of T_f vs composition

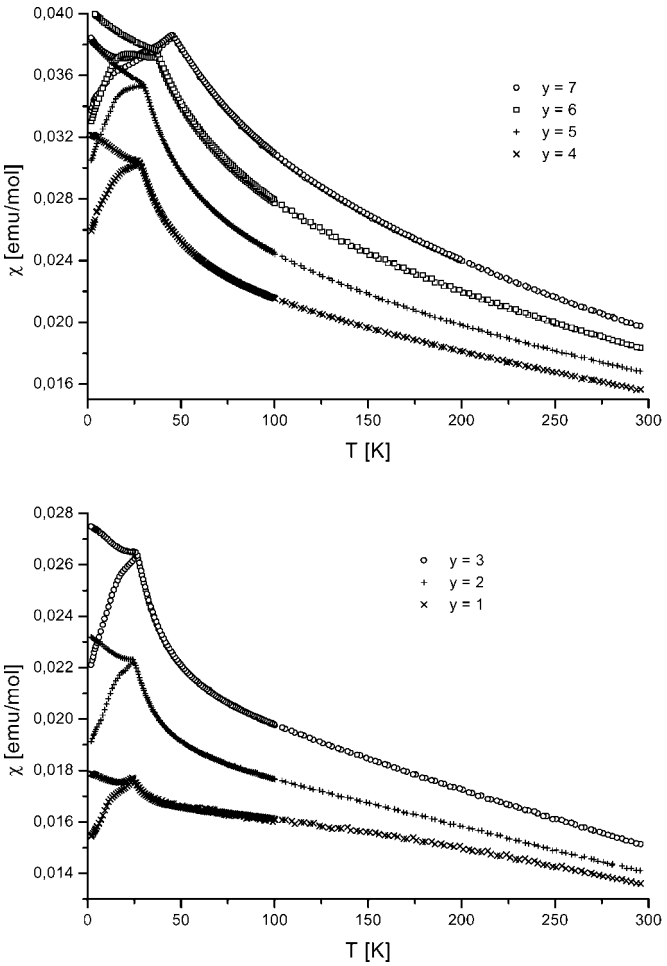

FIG. 4. The magnetic susceptibilities of the compounds $TlCr_5S_{8-y}Se_y$ ($y = 1$–7) in the temperature region between 4 and 300 K measured at 100 G.

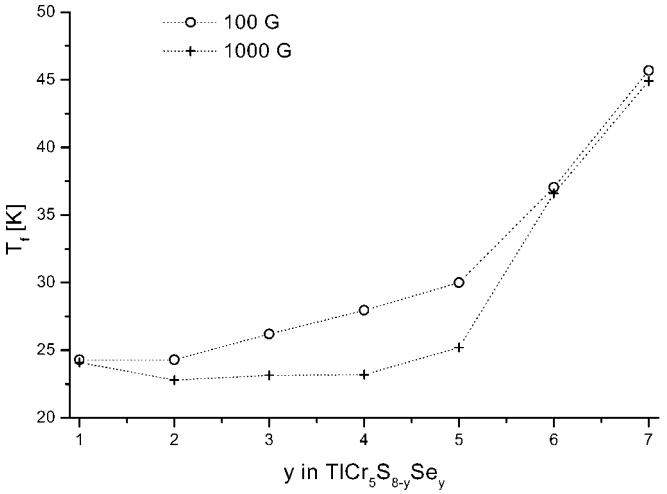

FIG. 5. The dependence of T_f [K] from the magnetic field and on function of composition. The dotted line serves as a guide for the eyes.

is obvious for the two regions $1 \leq y \leq 4$ and for $4 \leq y \leq 7$ (see Fig. 5).

Within the series $TlCr_5S_{8-y}Se_y$ the successive exchange of S by Se does not alter the magnetic part of the structure as the oxidation state of Cr remains constant. Hence, in all samples 5 Cr(III) atoms with a d^3 electronic configuration contribute to the magnetic behavior. Consequently, the significant alterations of the Cr–Cr distances as well as of the angles Cr–X–Cr introduced when S is replaced by Se must be responsible for the magnetic behavior observed. As discussed above a competition between direct antiferromagnetic exchange and ferromagnetic superexchange strongly influences the resulting magnetic properties. With increasing Se content the Cr–Cr interatomic distances are enlarged, but as was pointed out in our previous contribution not in a linear way as a consequence of the nonstatistical distribution of the S/Se atoms over the 4 different sites. Furthermore, the angles Cr–X–Cr being near 90° vary in a nonlinear fashion. But as anticipated in our previous work, there is no evidence for any crystallographic superstructure, i.e., ordering of the S or Se atoms in the S/Se lattice. Therefore, on a microscopic scale the Cr atoms experience locally different direct and indirect magnetic exchange interactions due to the nearly randomly distributed S/Se substructure. As was pointed out above, T_f increases when the Se content is raised (see Fig. 5). Taking also into account the evolution of the Weiss constant θ with composition it is obvious that in the S-rich samples direct Cr–Cr exchange dominates. What happens on a microscopic scale could be envisaged considering the different exchange paths denoted as J_F and J_{AF} in Fig. 3 and the scheme shown in Fig. 7. If the chalcogen positions joining Cr2 and Cr3 via the common face are fully occupied by S atoms the Cr–Cr distance is so short that a Cr_2 dimer in the antiferromagnetic ground state is formed. Such a dimer interrupts long-range exchange and suppresses the formation of a three dimensional spin structure (36). A part of the magnetic spin structure of $TlCr_5Se_8$ is displayed in Fig. 7. The magnetic moments have only components in the b direction and they may be treated as Ising spins. The arrangement is reminiscent of the plaquette of Ising spins used in the pioneering paper by Toulouse that introduces spin frustration (48). In the pure selenide all bond energies are satisfied and long-range ordering of the magnetic moments is observed. But it is obvious from Fig. 7 that the partial substitution of Se by S on $X(1)$ site joining the Cr2 atoms shortens the Cr2–Cr2 interatomic separation thus changing the formerly ferromagnetic exchange into a weak antiferromagnetic link. As a consequence the whole arrangement becomes frustrated leading to the observed spin–glass behavior. This interpretation is in full agreement with the X-ray crystal structure investigations demonstrating the high preference of Se for site $X(1)$ and with the trend of the paramagnetic Curie temperature discussed above.

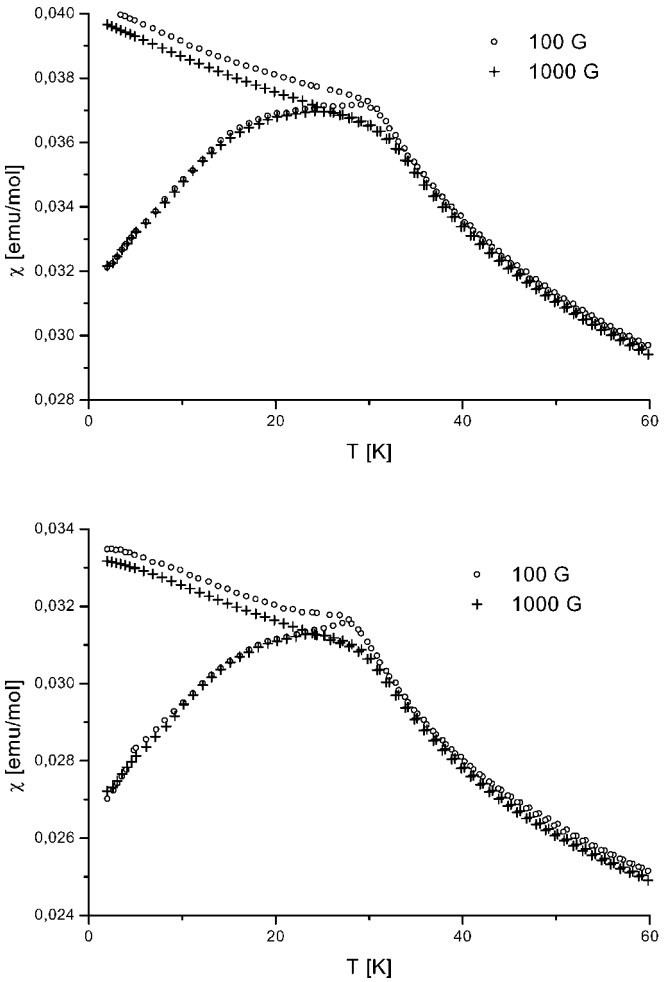

FIG. 6. Two examples of the field dependence of the magnetic susceptibilities near T_f: (top) $TlCr_5S_3Se_5$, (bottom) $TlCr_5S_4Se_4$.

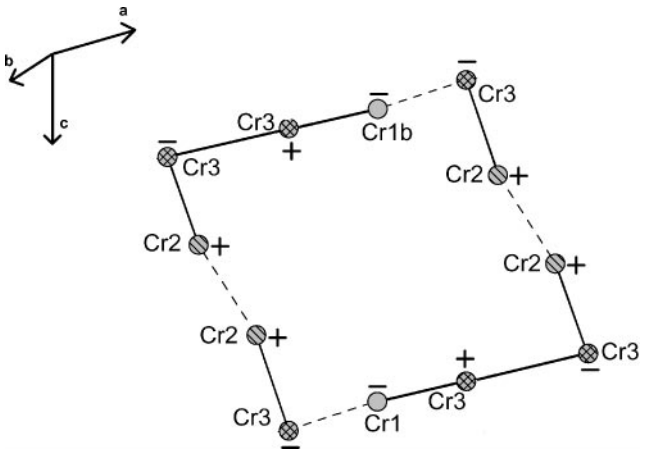

FIG. 7. Part of the magnetic structure of $TlCr_5Se_8$ determined at 2 K. *Note*: the + and − signs denote the directions of the spins parallel to the crystallographic *b* axis. The ferromagnetic links are marked by broken lines, the antiferromagneic interactions by full lines.

In metallic systems, indirect competing exchange interactions between moments located in different neighboring shells mediated by conduction electrons may lead to frustration due to the rapid spatial oscillation of the RKKY interaction. Preliminary investigations of the electrical properties of the different samples show semiconducting behavior with an increasing band gap as S content increases. Hence, the RKKY mechanism could be rejected.

It is also of interest that for $TlCr_5Se_2S_6$ and $TlCr_5SeS_7$ the susceptibility data show an appreciable scattering above about 100 K (see Fig. 8). In addition, for the members with $y = 1$ and 2 the curves exhibit a downward curvature clearly indicating that a Curie–Weiss-like behavior is not fulfilled (see Fig. 8). This behavior suggests that within the different domains Cr_2 dimers in the antiferromagnetic state dominate the magnetic properties because for the pure sulfide a temperature dependence of the magnetic susceptibility was observed, typical for a low-dimensional spin system (36).

C. Neutron Scattering Experiments

The neutron scattering experiments were conducted on $TlCr_5Se_2S_6$ at 300, 200, 120, 60, and 5 K. The results of the Rietveld refinement of the 300 K data set is in full agreement with the data obtained during our X-ray single crystal work. We note that the lattice parameters as well as the monoclinic angle β decrease in a linear way with falling temperature (Table 3).

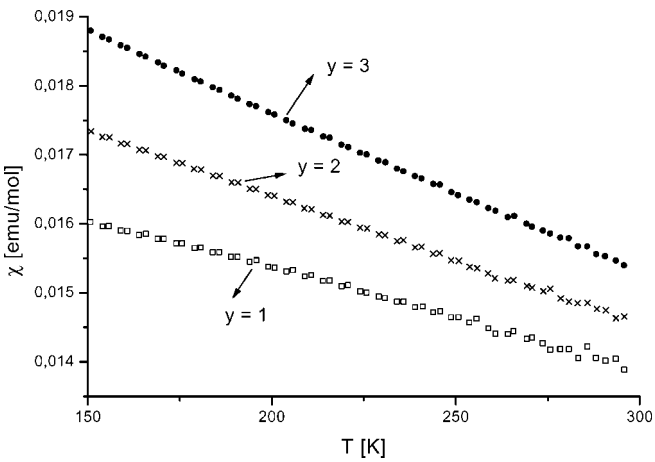

FIG. 8. The susceptibilities of $TlCr_5S_{8-y}Se_y$ ($y = 1$–3) above 150 K. Note the scattering of the data as well as the downward curvature for $y = 1$ and 2.

TABLE 3
Lattice Parameters for $TlCr_5Se_2S_6$ Obtained at Different Temperatures

	300 K	200 K	120 K	60 K	5 K
a [Å]	17.9570(4)	17.9358(4)	17.9188(4)	17.9062(5)	17.9009(4)
b [Å]	3.4694(1)	3.4665(1)	3.4645(1)	3.4631(1)	3.4624(1)
c [Å]	8.7166(2)	8.6988(2)	8.6849(2)	8.6791(3)	8.6792(2)
β°	105.143(2)	105.101(2)	105.056(2)	105.017(3)	104.999(2)

Note. The esd's are given in parentheses.

As can be seen in the difference powder patterns (see Fig. 9) no additional Bragg reflections occur down to 5 K due to long-range ordering of the magnetic moments. The most significant changes are observed in the d-value range 3–7 Å. With decreasing temperature the background starts to grow and a broad and nearly featureless modulation is seen at 5 K. The evolution of this "hump" starts at about 200 K and exhibits a continuous increase as can be seen in the difference curves (see Fig. 10). A rough estimate of the domain size using the Scherrer equation yields 15 Å.

A better insight into the short-range correlations can be obtained by transforming the data, using a Fourier transformation, as presented for example in (49, 50). The transformation gives the radial correlation function

$$F(r) = \int_{QI}^{Qh} I_d(Q) \cdot f(Q)^{-2} \cdot Q \sin(Qr)\, dQ,$$

where $Q = 4\pi \sin(\theta)/\lambda$ is the scattering vector, $I_d(Q)$ is the magnetic scattering intensity at Q, with the paramagnetic scattering subtracted, and $f(Q)$ is the magnetic form factor. Figure 11 shows the Fourier transformations of the three low-temperature data sets. The nearest Cr–Cr distances are indicated by the arrows. It is obvious that from 120 K down to 5 K the antiferromagnetic exchange becomes weaker and the ferromagnetic correlations increase with falling temperature. A shift of the positions of the higher coordination shells is also seen that may be caused by the significant alterations of interatomic distances. The main limitations in the analysis is most likely the limited Q range of the data.

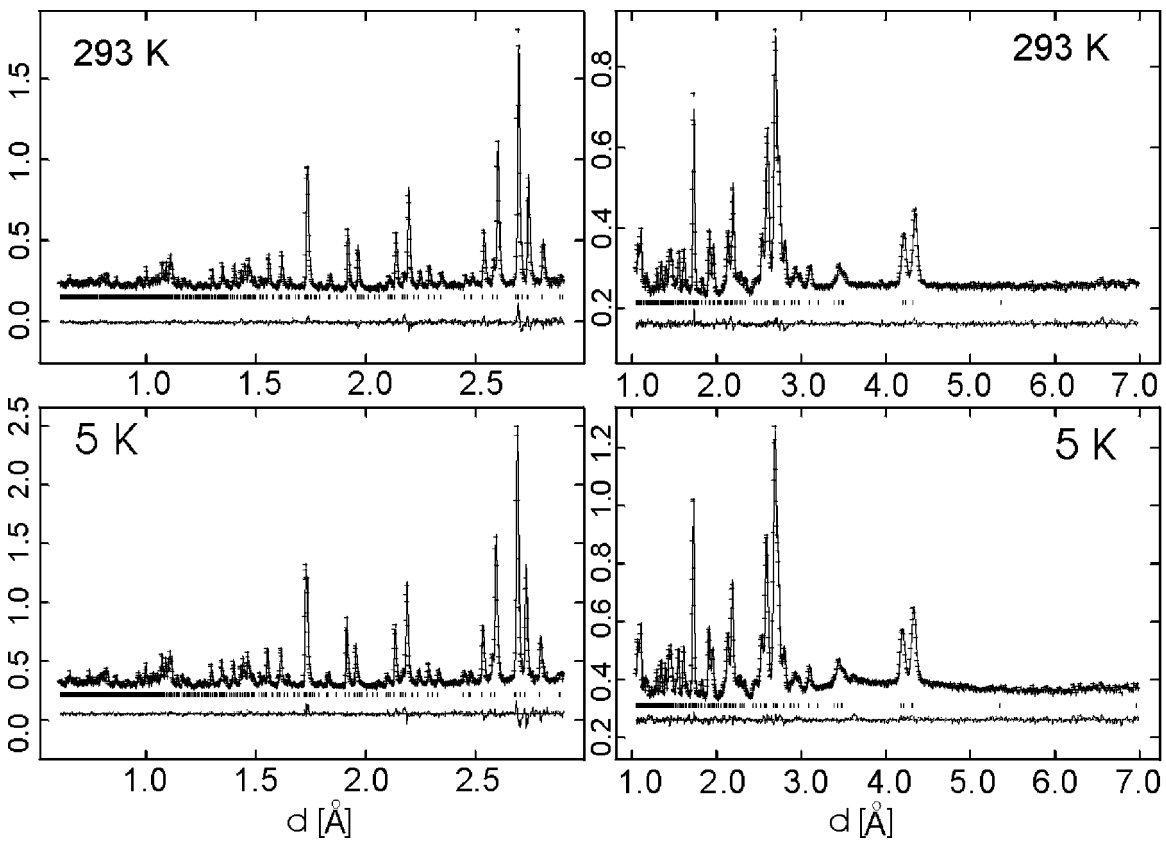

FIG. 9. Refined powder patterns recorded at (top) 293 K and at (bottom) 5 K. Difference curves are presented in the lower part of the patterns: (+) measured data, (—) refined profile, vertical bars represent the positions of the reflections. (Left patterns) back scattering regions; (right patterns) forward scattering regions. *Note*: the y axes show normalized counts.

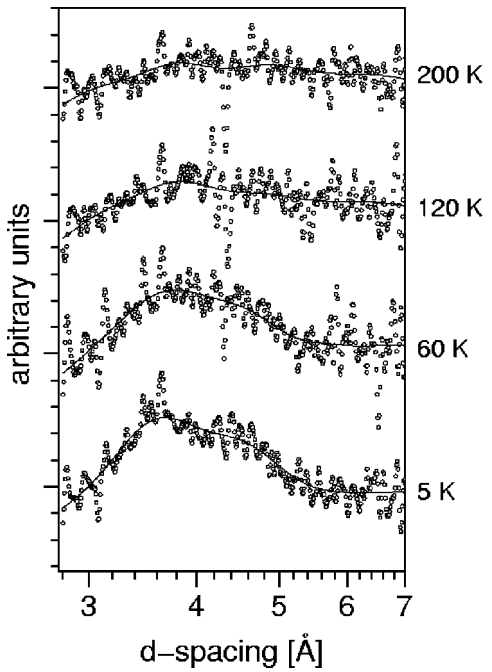

FIG. 10. $TlCr_5S_6Se_2$ powder patterns after substraction of the 300 K pattern. The solid line is the smoothed background.

We note that a peak with a very low intensity occurs at 200 K located at $d = 3.65$ Å. With falling temperature the intensity of this "reflection" exhibits only a minute increase. A simple explanation for the occurrence of this reflection is not at hand at the moment. Because the intensities of all reflections could be refined without considering any magnetic contributions, a development of magnetic long-range order as the reason for this reflection could be rejected.

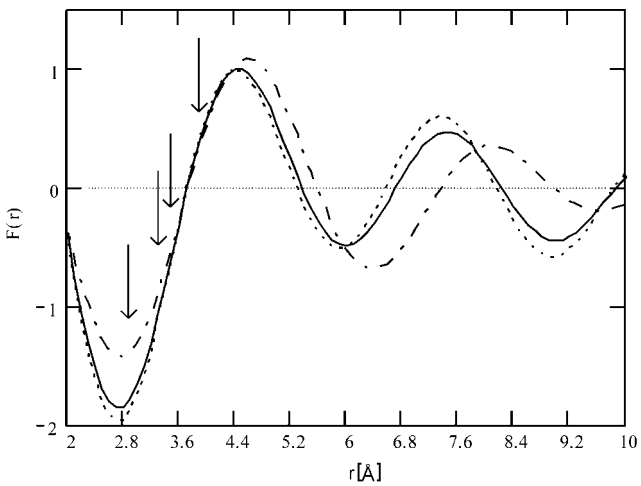

FIG. 11. Real-space radial correlation functions (arbitrary units) obtained by Fourier transformation of the low-temperature difference data sets. The arrows indicate the nearest-neighbor Cr–Cr distances: (–·–·–) 5 K, (—) 60 K, and (···) 120 K.

CONCLUSIONS

The members of the series $TlCr_5S_{8-y}Se_y$ with $y = 1$–7 exhibit spin frustration due to the non-magnetic anionic sublattice. In view of the magnetic properties of the two end members of this series ($y = 0$, 8) such a behavior for the mixed S/Se compounds is surprising and unexpected. Spin–glass behavior was reported for a large number of compounds in which magnetic cations are partially replaced by nonmagnetic cations thus suppressing magnetic long-range order. Spin frustration was also observed for compounds which are composed of cations with different electronic configurations such that direct or indirect exchange interactions do not lead to an ordered spin state. Therefore, to the best of our knowledge, the samples investigated here are the first examples of spin–glass behavior occurring in a system of identical magnetic cations embedded in a disordered, nonmagnetic anionic sublattice.

In the high-temperature region Curie–Weiss behavior is observed. The successive substitution of S by Se enhances the ferromagnetic 90°Cr–(S/Se)–Cr superexchange interaction at the expense of the direct Cr–Cr antiferromagnetic interactions. Consequently, the magnitude of the Weiss constant θ decreases with increasing Se content. The alterations of interatomic distances and angles by substitution of S by Se are not linear due to a slight preference of Se for two of the four crystallographic chalcogen sites, and two distinct regions, $0 \le y \le 4$ and $4 \le y \le 8$, can be distinguished. The magnetic properties reflect this nonlinearity, for example by the evolution of θ and the magnetic moment per Cr(III) with composition. Furthermore, Cr2–Cr3 distances (octahedron with common face) reach a critical value near the composition $TlCr_5S_4Se_4$. For samples with more sulfur this distance is so short that Cr_2 dimers are formed which are in an antiferromagnetic ground state. This assumption is supported by the significant deviation of the magnetic susceptibilities from the Curie–Weiss law above 100 K.

At low temperatures the competition between direct antiferromagnetic and indirect ferromagnetic exchange interactions leads to a spin–glass behavior, the freezing temperature T_f increasing with increasing Se abundance. Starting with the pure selenide, which is a three-dimensional antiferromagnet, the partial substitution of Se by S on the $X(1)$ site shortens the Cr2–Cr2 distance and alters the ferromagnetic exchange into a weak antiferromagnetic link leading to the observed spin–glass behavior. Neutron scattering experiments between 5 and 300 K clearly exclude the formation of long-range magnetic order. Below 120 K the neutron diffraction patterns exhibit a broad "hump" of magnetic scattering that swells with decreasing temperature.

The evolution of such a "short-range order" feature in the neutron diffraction patterns is a further indication for frustrated magnetic interactions and spin–glass behavior. Furthermore, the analysis of the magnetic scattering in terms of radial correlation functions supports the suggestion that with decreasing temperature the ferromagnetic exchange is enhanced whereas the antiferromagnetic interactions become weaker.

ACKNOWLEDGMENTS

Financial support by the State of Schleswig-Holstein as well as financial support of ROTAX by the BMBF under Contract KI5BO3 are gratefully acknowledged.

REFERENCES

1. H. Boller, K. O. Klepp, and K. Kirchmayr, *Mater. Res. Bull.* **30,** 365 (1995).
2. L. Fournes and M. Vlasse, *Rev. Chim. Miner.* **15,** 542 (1978).
3. J. Huster, *Z. Anorg. Allg. Chem.* **447,** 89 (1978).
4. J. Huster, *Z. Kristallogr.* **144,** 146 (1979).
5. R. Quint and H. Boller, *Mater. Res. Bull.* **22,** 1499 (1987).
6. K. D. Bronsema and J. Mahy, *Phys. Status Solidi A* **104,** 603 (1987).
7. N.-H. Dung, V.-V. Tien, H. J. Behm, and P. T. Beurskens, *Acta Crystallogr., Sect. C: Cryst. Struct. Commun.* **43,** 2259 (1987).
8. C. Platte and H. Sabrowsky, *Naturwissenschaften* **62,** 528 (1975).
9. T. D. Brennan and J. A. Ibers, *Mater. Res. Bull.* **27,** 231 (1992).
10. N. E. Brese and J. A. Ibers, *J. Solid State Chem.* **76,** 1 (1988).
11. K. Herudek, Ph.D. thesis, Aachen, 1993.
12. W. Bronger, C. Herudek, J. Huster, and D. Schmitz, *Z. Anorg. Allg. Chem.* **619,** 243 (1993).
13. T. Novet, M. Wagner, M. Jiang, and D. C. Johnson, *Mater. Res. Bull.* **30,** 65 (1995).
14. T. Ohtani,Y. Sano, K. Kodama, S. Onoue, and H. Nishihara, *Mater. Res. Bull.* **28,** 501 (1993).
15. S. Petricek, H. Boller, and K. O. Klepp, *Solid State Ionics* **81,** 183 (1995).
16. J. Garch, F. Boucher, M. Evain, C. J. O'Connor, and S. Li, *J. Solid State Chem.* **122,** 41 (1996).
17. W. Bensch and E. Wörner, *Solid State Ionics* **58,** 275 (1992).
18. W. Bensch and E. Wörner, *Mater. Sci. Forum* **133–136,** 659 (1993).
19. W. Bensch, E. Wörner, M. Muhler, and U. Ruschewitz, *Eur. J. Solid State Inorg. Chem.* **30,** 645 (1993).
20. R. Schöllhorn, Intercalation reactions of solids by electron/ion transfer, *in* "Proc. of Intern. Conf.: Phys. Intercal. Comp. Conf.," Trieste, Italy, Vol. 6–10, p. 33, 1981.
21. R. Schöllhorn, *Angew. Chem.* **92,** 1015 (1980).
22. W. Schramm, R. Schöllhorn, H. Eckert, and W. Müller-Warmuth, *Mater. Res. Bull.* **18,** 1283 (1983).
23. T. Ohtani and S. Onoue, *J. Solid State Chem.* **59,** 324 (1985).
24. H. Nishihara, T. Ohtani, and S. Onoue, *Europhys. Lett.* **8,** 189 (1989).
25. H. Nishihara, S. Onoue, T. Ohtani, and H. Yasuoka, *J. Magn. Mater.* **70,** 225 (1987).
26. W. Bensch, E. Wörner, and P. Hug, *Solid State Commun.* **86,** 165 (1993).
27. W. Bensch, O. Helmer, and C. Näther, *J. Solid State Chem.* **127,** 40 (1996).
28. W. Bensch, B. Sander, O. Helmer, C. Näther, F. Tuczek, A. Panich, and A. Shames, *J. Solid State Chem.* **145,** 235 (1999).
29. W. Bensch, O. Helmer, C. Näther, and M. Muhler, *J. Solid State Chem.* **145,** 247 (1999).
30. W. Bensch, O. Helmer, J. Lu, G. Wortmann, H.-J. Hesse, M. Kraus, and K. Lüders, *J. Solid State Chem.* **119,** 147 (1995).
31. W. Bensch and E. Wörner, *Mater. Res. Bull.* **28,** 1005 (1993).
32. W. Bensch, E. Wörner, and M. Muhler, *Mater. Res. Bull.* **29,** 155 (1993).
33. W. Bensch, E. Wörner, and F. Tuczek, *Mater. Res. Bull.* **30,** 1065 (1995).
34. W. Bensch, O. Helmer, and F. Tuczek, *Z. Kristallogr. Suppl.* **9,** 142 (1995).
35. C. Näther, O. Helmer, and W. Bensch, *Z. Kristallogr. Suppl.* **11,** 90 (1996).
36. W. Bensch, E. Wörner, M. Muhler, and U. Ruschewitz, *J. Solid State Chem.* **110,** 234 (1994).
37. T. Ohtani and S. Onoue, *Mater. Res. Bull.* **21,** 69 (1986).
38. W. Bensch, B. Sander, C. Näther, I. Jeß, and O. Helmer. *Z. Anorg. Allg. Chem.* **625,** 83 (1999).
39. W. Kockelman, M. Meißner, H. Heinen, A. Kirfel, and W. Schäfer, *Mater. Sci. Forum* **321–324,** 332 (2000).
40. A. C. Larson and R. B. Von Dreele, "FSAS: General Structure Analysis System," Report LAUR 86–87, Los Alamos Laboratory, Los Alamos, NM, 1986.
41. J. B. Goodenough, *J. Phys. Chem. Solids* **6,** 287 (1958).
42. J. B. Goodenough, *Phys. Rev.* **100,** 564 (1955).
43. J. Kanamori, *J. Phys. Chem. Solids* **10,** 87 (1959).
44. R. J. Bouchard, P. A. Russo, and A. Wold, *Inorg. Chem.* **4,** 685 (1965).
45. P. Colombet and M. Danot, *J. Solid State Chem.* **45,** 311 (1983).
46. D. A. Odink, V. Carteaux, C. Payen, and G. Ouvrard, *Chem. Mater.* **5,** 237 (1993).
47. W. Bensch, C. Näther, O. Helmer, and C. Ritter, *J. Alloys Comp.* **290,** 41 (1999).
48. G. Toulouse, *Comm. Phys.* **2,** 115 (1977).
49. P. Colombet, M. Danot, and J. L. Soubeyroux, *J. Magn. Magn. Mater.* **51,** 257 (1985).
50. J. N. Reimers, J. E. Greedan, R. K. Kremer, E. Gmelin, and M. A. Subramanian, *Phys. Rev. B* **43,** 3387 (1991).
51. M. Rosenberg, A. Knülle, H. Sabrowsky, and Chr. Platte, *J. Phys. Chem. Solids* **43,** 87 (1982).
52. S. Jobic, F. Bodenan, G. Ouvrard, E. Elkaim, and J. P. Lauriat, *J. Solid State Chem.* **115,** 165 (1995).
53. S. Yuri, S. Ohta, S. Anzai, M. Aikawa, and K. Hatakeyama, *J. Magn. Magn. Mater.* **70,** 215 (1987).
54. A. Lafond, A. Meerschaut, J. Rouxel, J. L. Tholence, and A. Sulpice, *Phys. Rev. B* **52,** 1112 (1995).
55. A. Meerschaut, A. Lafond, L. M. Hoistad, and J. Rouxel, *J. Solid State Chem.* **111,** 276 (1994).
56. R. E. Marsh, *J. Solid State Chem.* **77,** 190 (1988).